JOURNAL OF GEOPHYSICAL RESEARCH, VOL. 100, NO. A7, PAGES 12,075–12,092, JULY 1, 1995

The double oval UV auroral distribution 1. Implications for the mapping of auroral arcs

R. D. Elphinstone,[1] J. S. Murphree,[1] D. J. Hearn,[1] L. L. Cogger,[1] I. Sandahl,[2] P. T. Newell,[3] D. M. Klumpar,[4] S. Ohtani,[3] J. A. Sauvaud,[5] T. A. Potemra,[3] K. Mursula,[6] A. Wright,[7] and M. Shapshak[8]

Abstract. During the later stages of the auroral substorm the luminosity distribution frequently resembles a double oval, one oval lying poleward of the normal or main UV auroral oval. We interpret the double oval morphology as being due to the plasma sheet boundary layer becoming active in the later stages of the substorm process. If the disturbance engulfs the nightside low-latitude boundary layers, then the double oval configuration extends into the dayside ionospheric region. The main UV oval is associated with the inner portion of the central plasma sheet and can rapidly change its auroral character from being diffuse to discrete. This transition is associated with the substorm process and is fundamental to understanding the near-Earth character of substorm onset. On the other hand, the poleward arc system in the nightside ionosphere occurs adjacent to or near the open-closed field line boundary. This system activates at the end of the optical expansion phase and is a part of the recovery phase configuration in substorms where it occurs. These two source regions for nightside discrete auroral arcs are important in resolving the controversy concerning the mapping of arcs to the magnetosphere. The dayside extension of this double oval configuration is also investigated and shows particle signatures which differ considerably from those on the nightside giving clues to the magnetospheric source regions of the aurora in the two local time sectors. Near-Earth substorm onsets are shown to be coupled to processes occurring much further tailward and indicate the importance of understanding the temporal development of features within the double oval. Using "variance images," a new technique for the investigation of these dynamics is outlined.

1. Introduction

The question of where auroral arcs map to in the magnetosphere is a long standing problem. One view advocated by *Feldstein and Galperin* [1985] maps these arc systems to the entire central plasma sheet and associates the plasma sheet boundary layer (PSBL) with purely diffuse auroral precipitation. The other view places surges and discrete aurora adjacent to the open-closed field line boundary within the PSBL [e.g., *Burke et al.*, 1994; *Lyons*, 1991]. The central plasma sheet is then associated with the more equatorward diffuse precipitation. *Lui* [1977] equates the central plasma sheet with the diffuse precipitation but places the discrete aurora in the poleward portion of this region. *Lui* [1977, p. 2224] concludes the discrete aurora has a source "within but often near the poleward boundary of the plasma sheet." This latter paper is an example of the view which existed before the the PSBL came to be associated with the low-altitude boundary plasma sheet (BPS). The original view of the low-altitude boundary plasma signature (originally designated boundary plasma layer or BPL), which was put forth by *Winningham et al.* [1975], was developed before the introduction and definition of the PSBL at high altitude. The confusion between the high-altitude PSBL and the low-altitude BPS has led many researchers to make an identification and correspondence between the two regions. This paper is an attempt to reconcile these diverse views by investigating an auroral configuration which we term the double oval distribution.

As the aurora ceases its poleward progression, which characterizes the expansion phase, the aurora within the bulge often fades noticeably. From magnetometer data, it is known that at this time the westward electrojet can divide into two separate electrojets and that the fading of the aurora can correspond to a local recovery of an *H* bay there [*Elphinstone et al.*, 1993; *Kotikov et al.*, 1993]. Therefore the beginning of the recovery phase at least locally is associated with the obvious fading of

[1] Department of Physics and Astronomy, University of Calgary, Calgary, Canada.
[2] Swedish Institute for Space Physics, Kiruna, Sweden.
[3] Applied Physics Laboratory, Johns Hopkins University, Laurel, Maryland.
[4] Space Science Laboratory, Lockheed Missiles and Space Company Incorporated, Palo Alto, California.
[5] Toulouse University, Toulouse, France.
[6] Department of Physical Sciences, University of Oulu, Oulu, Finland.
[7] Mathematical Institute, University of St. Andrews, St. Andrews, Fife, Scotland.
[8] Institute of Plasma Physics, Kungliska Tekniska Hogskolan, Stockholm, Sweden.

Paper number 95JA00326.
0148-0227/95/95JA-00326$05.00

the aurora within the bulge once the expansion has reached its poleward limit. Auroral patterns which occur during the late stages of substorm development will be the focus of this paper. These patterns will collectively be identified as the double oval distribution.

This paper will address the problem of mapping this distribution by studying both high- and low-altitude satellite data in conjunction with Viking auroral image data at times when the double oval distribution is observed. The next section of this paper deals with common patterns observed during a double oval auroral configuration. Section 3 compares the double oval as seen in the UV with other data sets recorded by Viking, DMSP, and CCE. In this section a new technique for investigating the dynamics of the aurora is demonstrated. Section 4 shows that a coupling can exist between the two regions of the double oval which can lead to a substorm onset. The last section is a summary of the findings in this paper. A companion paper [*Elphinstone et al.*, this issue] investigates in more detail the temporal development of the most poleward arc system and demonstrates the association of it with the PSBL and wave phenomena.

2. Elements of the Auroral Substorm Recovery Phase Development as Observed From Viking

Figure 1 illustrates three auroral patterns which exist in the late stages of substorm development. These are all associated with what we call the double oval distribution. In a given substorm one or more of these patterns may appear and the order of the patterns varies. We shall use the following as a definition of the double oval configuration: An auroral distribution which has two distinct auroral arc systems at different latitudes which span several hours of magnetic local time around midnight. Between these two distinct systems there may be other discrete features which locally hide this larger scale pattern. The patterns shown in Figure 1 are schematics based on the viewing of approximately 45000 Viking images acquired during 1986. Individual events however can also be found within the data set which correspond very well with the given schematics presented here. The schematics therefore are composites which represent reasonably well the general case while also accurately portraying specific individual events.

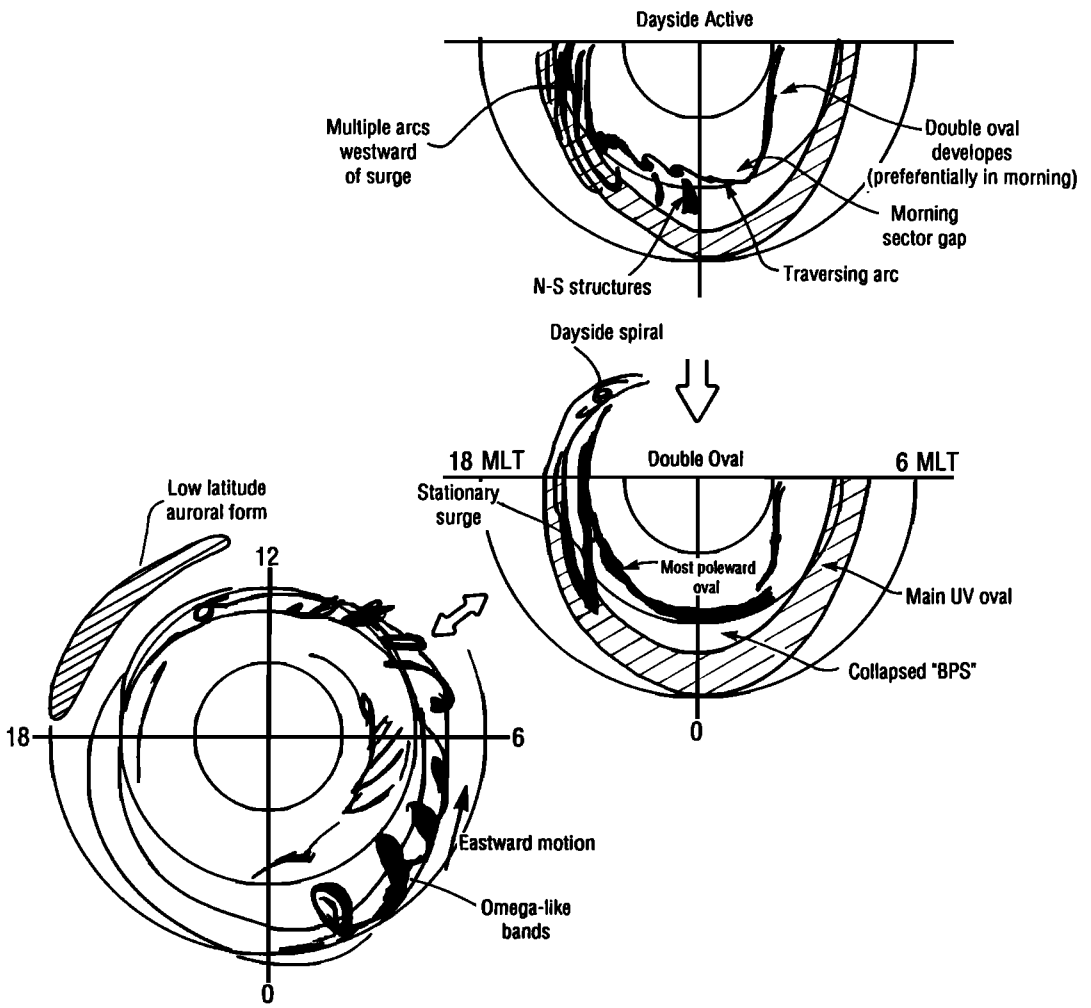

Figure 1. Three recovery phase luminosity distributions. The top panel illustrates the formation of the double oval in the dawn sector, vortex streets, and multiple arcs west of the bulge. The middle panel shows the dusk sector manifestation of the double oval and the bottom panel shows the pattern typical when omega bands exist in the early morning. These panels form modules which can be put in series or superposed to give an auroral sequence during substorm recovery phase.

Figure 1 indicates that on occasion the double oval represents two separate large-scale regions which can extend to within a few hours of local noon (see middle panel near 14-15 MLT and bottom left panel near 10 MLT) [*Elphinstone and Hearn*, 1992; *Elphinstone et al.*, 1993]. Further, while there are many localized discrete forms within this distribution it is the extended local time nature of the two main distributions which leads to the characteristic double oval configuration. This distribution has been seen in ISIS 2 observations [*Murphree et al.*, 1981, Figure 6]. It can also be clearly seen in other global images of the auroral distribution [e.g., *Kamide and Akasofu*, 1975; *Craven and Frank*, 1987; *Pellinen et al.*, 1992]. The most equatorward distribution or the main UV oval is the portion of the distribution which was found to map to the inner portion of the central plasma sheet by *Elphinstone et al.* [1991].

In the initial stages of the double oval development, activity tends to be limited to the region near midnight. At this time multiple arcs can be seen to the west of the surge form [*Nielsen et al.*, 1993]. At the poleward edge of the substorm bulge intensifications occur and multiple spirals appear and disappear. These tend to develop coherently over several hours local time centred around the midnight meridian. In the magnetotail the formation of these spiral forms can coincide with the recovery of the plasma sheet at ISEE distances [*Cogger and Elphinstone*, 1992]. This sudden intensification of the poleward arc system near midnight has been called the "traversing arc" [*Murphree and Elphinstone*, 1988]. Features within the bulge which are aligned from northwest to southeast also develop at this time [*Nakamura et al.*, 1993]. This auroral pattern is represented by the top panel in Figure 1.

High-latitude arc systems can form in the dawn and dusk sectors (Figure 9 in the work by *Elphinstone et al.* [1993]) and large scale stationary surge systems can form in the evening sector. This results in the configuration shown in the middle panel of Figure 1. The relation of the stationary surge to the dayside distribution has also been illustrated in this panel as well as the location of the collapsed BPS as described by *Winningham et al.* [1975]. The Viking images show that omega bands originate on the main UV oval (the bottom left panel of Figure 1) and so occur during times when the inner portion of the plasma sheet is active [e.g., *Elphinstone et al.*, 1993; *Pellinen et al.*, 1992].

Plate 1 shows the auroral configurations during six intervals on April 9 and 10, 1986, marked in the AL diagram (Figure 2).

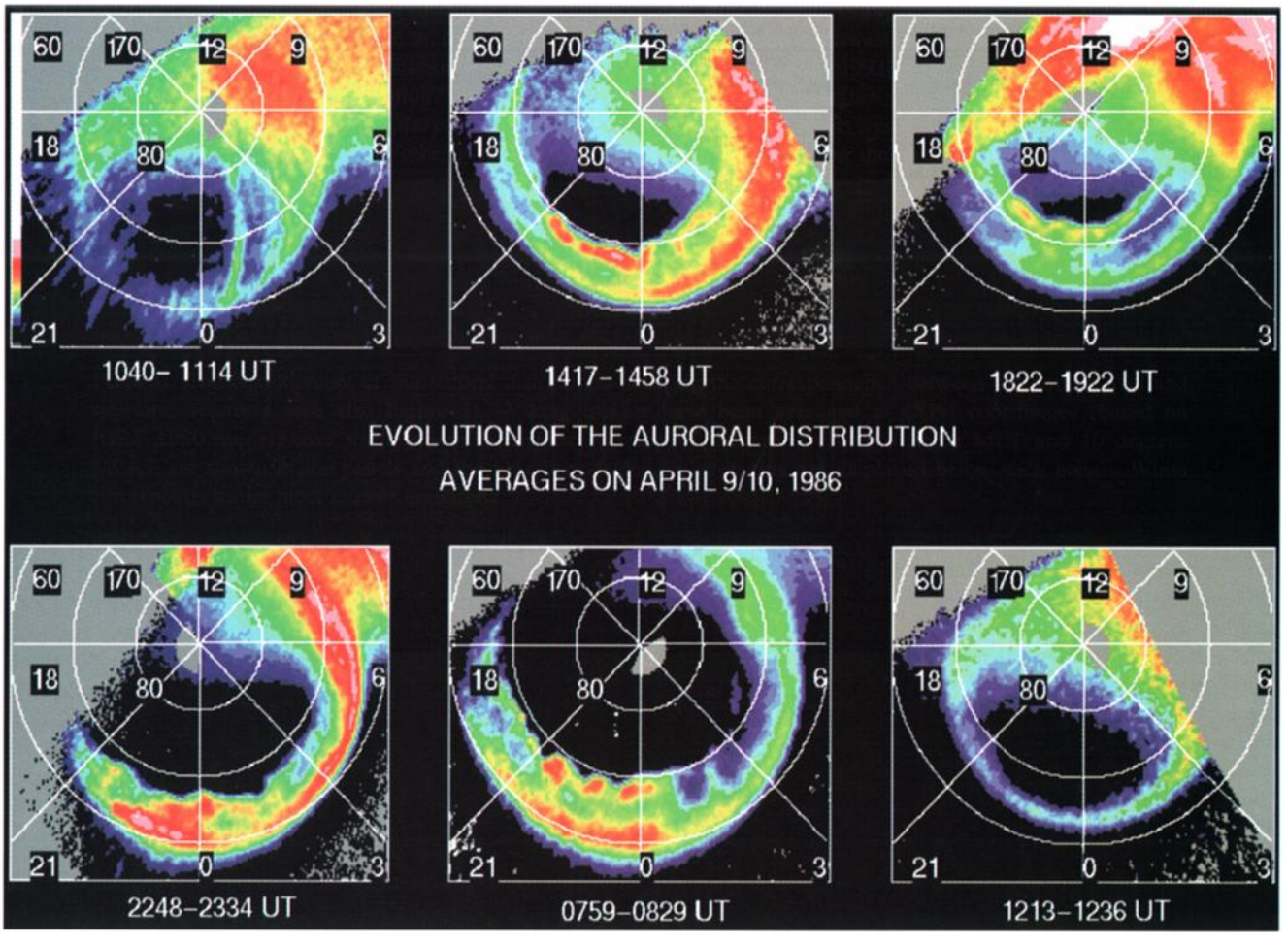

Plate 1. The development of the auroral distribution showing the correspondence between the double oval and substorm recovery (see also Figure 2). Viking images have been averaged in CGM coordinates (based on IGRF 1980 model) over the northern hemisphere portion of the orbit. Every 3 hours MLT and 10 degrees MLAT are shown in the panels and the time periods for the averaging are displayed below each panel. White corresponds to the most intense emissions.

This Plate illustrates the connection between recovery phase and the double oval distribution. This 2-day period was chosen since there were many separate recovery phases recorded by the Viking imager. Since Viking has about a 4-hour orbital period and viewing times are restricted to when the satellite passes over the northern hemisphere auroral distribution, it is not often that a 32-hour time interval yield several separate recovery phase observations. This time interval was chosen simply for that reason.

It is generally difficult to convey in a single plate the image data associated with hours worth of observations. Thus, in order to illustrate the general configurations of the aurora, averages were constructed. These consisted of transforming the individual images as viewed from the satellite perspective into a pixel map corresponding to Corrected Geomagnetic coordinates (CGM80). Each pixel in the original data was assigned a specific pixel location on the CGM image grid defined by the viewing geometry and by assuming an emission height of 120 km altitude. When multiple pixels from the original data corresponded to a given pixel location on the CGM image, the corresponding data number intensities were averaged together and the average was associated with the particular CGM pixel element. CGM transformed images of data number intensity could then be constructed from the original data. In order to get a good "average image" over the interval in question, all available images were first viewed and only those which were of good quality were selected for the transform process. These "CGM images" were then further processed by averaging together similar CGM pixel locations at all available times. This produced a CGM averaged image for a given time interval. Plate 1 shows six such averages corresponding to six Viking passes over the northern hemisphere aurora.

The upper left panel shows an *AL* quiet time distribution with a dawn sector polar arc. The other upper two panels show typical double ovals during substorm recovery. The bottom left panel of Plate 1 illustrates a transition time period where a new substorm onset is beginning from the peak in the main UV oval. This represents an expansion occurring during the recovery phase of a previous substorm (consistent with the *AL* index). The bottom middle panel of Plate 1 illustrates an *AL* recovery condition where both substorm regions are active. In this case both the most poleward system and the main UV oval are active regions for structured auroral arcs. The intensifications are occurring simultaneously but appear to be optically independent of one another. Finally in the bottom right panel of Plate 1, the aurora and the *AL* index (Figure 2) have returned to a quiescent state.

The double oval examples given above are specific cases of a more general trend concerning this distribution. A study was made of Viking image data combined with the *AL* index covering a two week period beginning on March 15, 1986. This consisted of approximately 60 hours of observing time, 63 satellite passes or about 3500 images. The *AL* index could be divided according to whether the *AL* was in recovery or not and similarly the image data could be used to determine whether or not a double oval distribution existed. Of the 38 separate intervals of *AL* recovery which were found, approximately 82% coincided with the existence of a double oval distribution. However, seven recovery time periods were found in which there was no evidence for this distribution. Nothing obvious was different about the *AL* index for these seven cases.

During this 2 week period there were 29 separate imaging intervals which were not during substorm *AL* recovery. Of these periods only three intervals showed the double oval configuration (i.e., 92% of these did not show the distribution). Two of these intervals occurred when the *AL* index was less than 50 nT but were within two hours of a previous substorm. These results show that while the double oval distribution is generally an *AL* recovery phase phenomenon, there are events where this simple classification scheme breaks down.

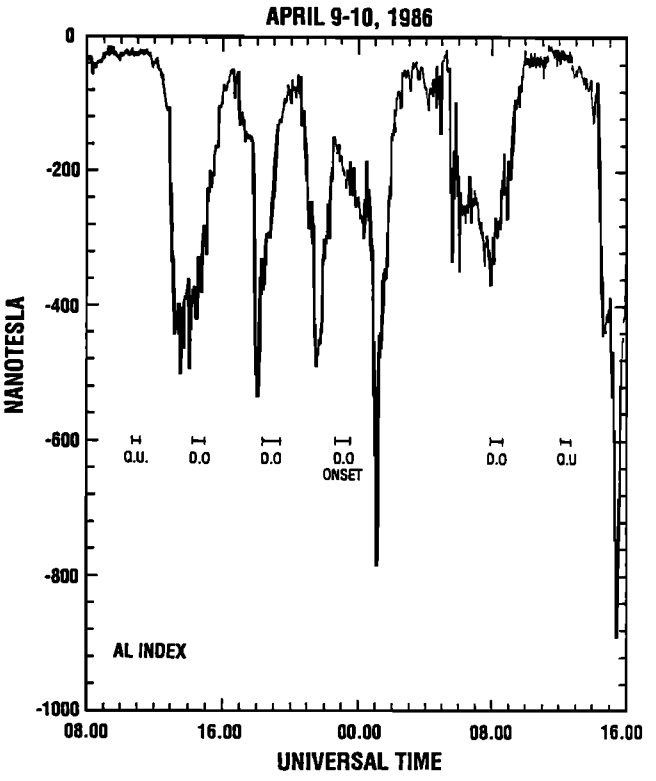

Figure 2. The *AL* index (provisional) for the 32 hour interval shown in Plate 1. The short horizontal segments show intervals in which Viking observations were available. Q.U. represents a quiet auroral distribution and D.O. means a double oval was observed.

3. Double Oval Dynamics and Particle Signatures

In this section two auroral events will be studied, one in the morning (event A) and the other in the evening and dayside sectors (event B). The morning sector event covers the substorm expansion and recovery phases and illustrates the locations of auroral activations relative to particle observations from the low altitude Viking spacecraft and the high altitude CCE satellite. We shall also introduce in this section a novel technique for the investigation of auroral dynamics. The second event illustrates the local time dependence of the double oval particle signatures based on the DMSP low altitude satellites. We shall first investigate the changes in the auroral distribution and then study the in situ satellite data.

Morning Sector Double Oval

Auroral distribution. Plate 2 shows an auroral configuration on July 27, 1986, at a time when the Viking satellite flew over the 3-4 MLT sector approximately coincident with the time that CCE encountered the inner edge of the central plasma sheet. The *AL* index showed a sharp decrease at 2042 UT indi-

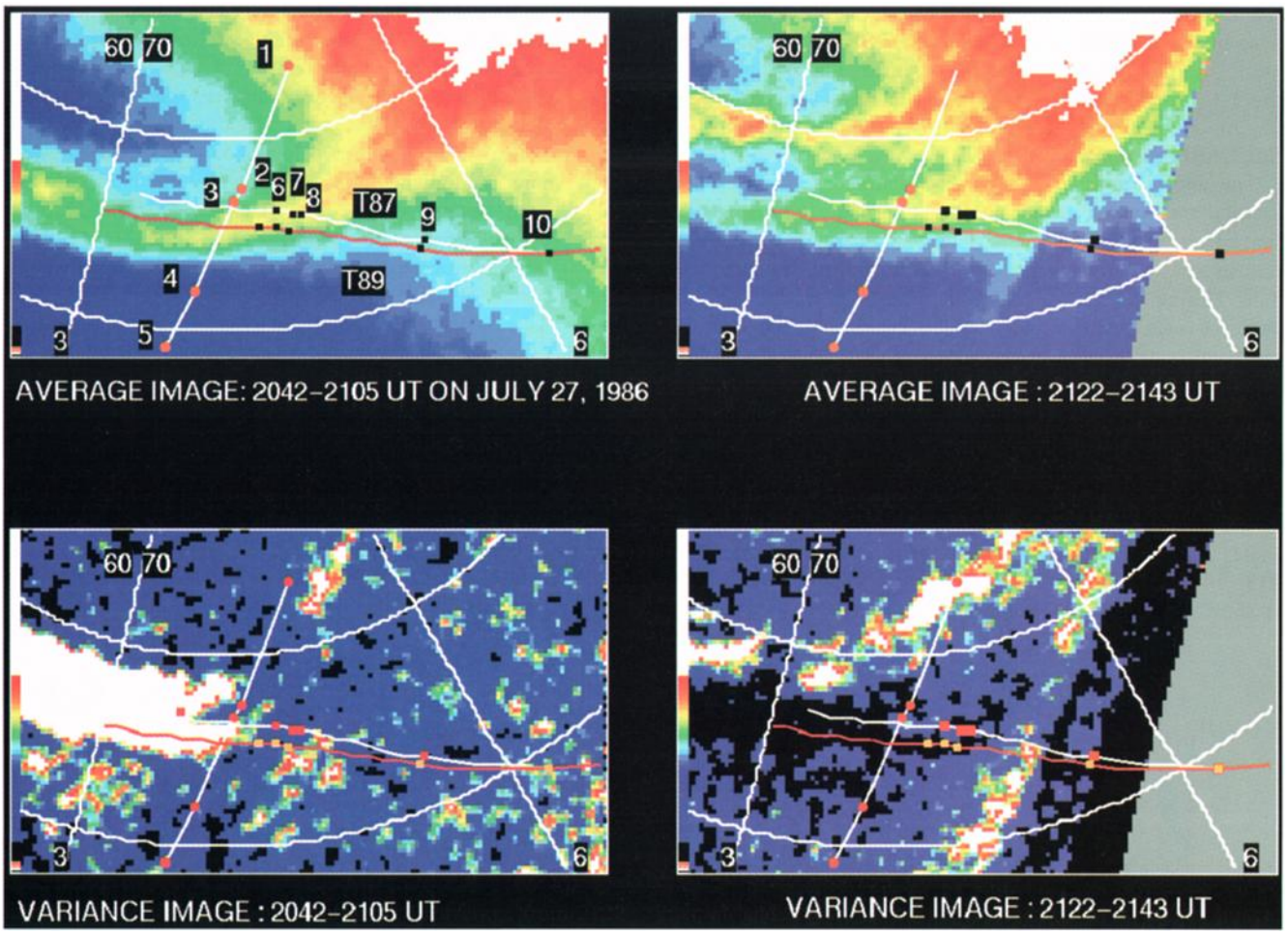

Plate 2. Viking and CCE trajectories superimposed on Viking auroral data. The top panels show average auroral configurations during (left) substorm expansion phase and (right) recovery phase. The bottom panels show images constructed from the standard deviations of the average images. White corresponds to the most intense emissions or largest variation. Points 1 to 5 show locations along the Viking satellite trajectory at 2123, 2135, 2136:10, 2143, and 2147 UT respectively. Points 6 to 10 show the ionospheric projections of the points along the CCE orbit at 1910, 1930, 1940, 2120, and 2200 UT respectively. The T87 model projection is shown in white while the T89 version is given in red. Also shown are the 3 and 6 MLT meridians (CGM 1980) and 60, 70 Mlat.

cating a substorm expansion phase had begun. This was consistent with an explosive onset seen in the auroral data. This index reached a minimum near -300 nT and began to recover by about 2105 UT. It continued to recover until a new explosive onset was seen in the auroral data at 2143 UT.

The top panels of Plate 2 show the average auroral distributions during these expansion (left panel) and recovery (right panel) phases. The distribution in the left panel has been averaged using images acquired between 2042 and 2105 UT (21 images) while the right panel represents an average from 2122 to 2143 UT (11 images). During expansion phase (top left panel) the most poleward region is relatively dim whereas during recovery phase (top right panel) this region becomes active and forms the double oval pattern. The Viking satellite trajectory has been projected to 120 km altitude and the CGM coordinates have been plotted in each panel of Plate 2. This line has points marked on it corresponding to particular signatures seen at the satellite (points 1 to 5). Also shown in all of the panels are the projections of the CCE satellite using two separate magnetic field models.

The bottom panels of Plate 2 are images constructed from normalized standard deviations of the average images. Each averaged pixel element has associated with it a standard deviation. Essentially the maps shown are images of these standard deviation maps. They have, however, been further normalized by the expected Poisson statistics standard deviation for each pixel. This latter step helped to eliminate dayglow contamination to these images. This technique of producing "variance images" is a novel means of extracting the dynamics of an interval and allows it to be represented in a single image. These images of "variance" illustrate where the aurora is most spatially and temporally active during expansion and recovery phases. This allows in a single image a method for illustrating the regions of dynamic aurora over some time interval. This is something which is difficult to show even using a large number of images displayed together.

In the neural network described by *Newell et al.* [1991], used to analyze particle data, the particle low-altitude boundary plasma sheet (LABPS) is typically characterized by temporally and/or spatially varying electron precipitation in the keV energy

range. Thus the dynamic UV aurora represented by these variance images is likely to be labeled as LABPS by the neural network (the UV camera is also most sensitive to precipitation in the 1 to 5 keV range). These variance images therefore allow an important means of producing two-dimensional images of this LABPS-like region.

The upper panels of Plate 2 show the change of the auroral distribution from an expansion phase morphology (left panel) to that of recovery (right panel). The bottom panels illustrate that fundamentally different regions activate during the two intervals. During expansion phase, the region near the main UV oval activates, while in recovery this region is inactive and the most poleward system becomes active. The following subsection outlines how these active regions correspond to low and high altitude satellite data.

Particles, convection and field-aligned currents. Plate 3 shows the time-energy particle spectrogram associated with the Viking trajectory marked in Plate 2. The electrons are shown in the top panel and ions in the lower panel. Points 1 to 5 in Plate 2 correspond respectively to the times 2123, 2135, 2136:10, 2143, and 2147 UT. The pitch angle of the particles is shown at the bottom of the plate. The band across the electrons at one keV and below is an instrument effect. Using a more detailed plot of the spectra, the following descriptions apply to the electrons for this event: (1) 2122 - 2123 UT: Low energy (less than 1 keV) electrons exist in this region. These occur poleward of any UV arcs seen by the imager. (2) 2123 - 2137 UT: Structured electrons below about 1 keV. These tend to be more field-aligned than the previous interval. Several field-aligned beams occur during the interval from 2125 to 2128 UT (one strong one is seen just after 2127 UT). (3) 2127 - 2140 UT: Unstructured electrons of about 1-7 keV in energy (i.e., electrons are isotropic except for an empty upgoing loss cone). This is the definition used by *Sandahl and Lindqvist* [1990]. (4) 2135: An inverted-V event with acceleration to about 7 keV. Equatorward of this point the electron fluxes begin to decrease, disappearing first at the higher energies. (5) 2140 - 2143 UT: Trapped, unstructured electrons.

Similarly, the ions show the following: (1) 2124 - 2130 UT: Ion conics are seen. (2) 2125 - 2128 UT: Precipitating ions in the 4 to 20 keV range are seen. A weak velocity dispersed ion signature (VDIS) during this interval (the highest energies occur at the highest latitude). This can be seen more clearly in a detailed spectrogram of this time interval. (3) 2128 - 2137 UT:

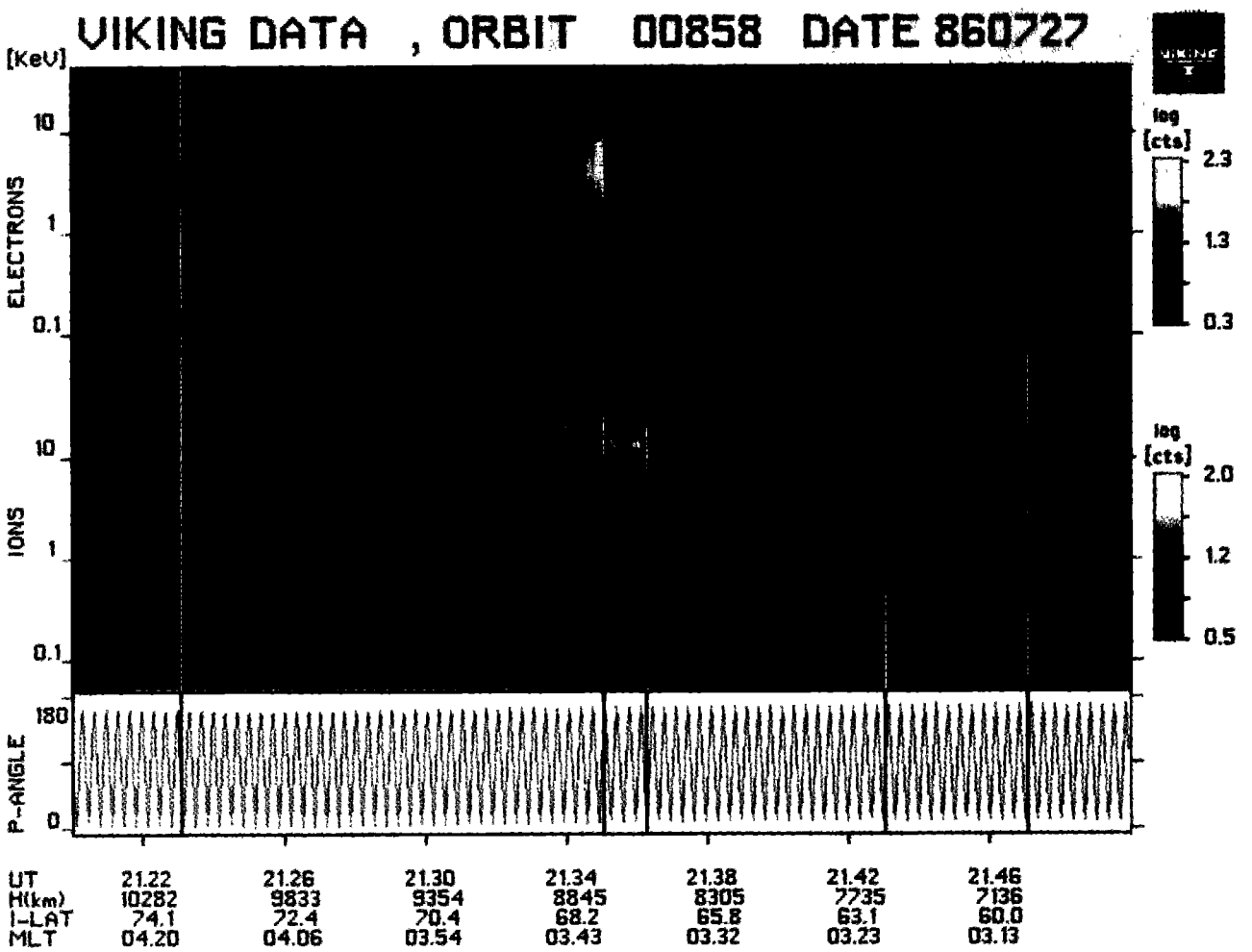

Plate 3. Viking energy-time particle spectrogram for the event shown in Plate 2 on July 27, 1986. Electrons are shown in the top panel and ions in the bottom panel. The colors correspond to accumulated counts in 32 separate energy channels (pitch angle resolution of ≈5°). An inverted V event can be seen at 2135 UT colocated with the main UV auroral oval in Plate 2. Red corresponds to the most intense fluxes. Vertical lines have been drawn to correspond with the points along the Viking trajectory shown in Plate 2.

Unstructured isotropic ions which have higher energy at lower latitudes. (4) 2136:10 - 2147 UT: Trapped ions and two separate overlapping dispersion signatures are seen. One extends between about 2137 and 2140 UT while the other occurs approximately from 2137 to 2143 UT. These ions decrease in energy with decreasing latitude. The boundary between isotropic ions and trapped ions with energies between 39 and 49 keV occurs at 2136:10 UT.

The peak in the energy flux into the ionosphere for both ions and electrons coincides approximately with the location of the inverted-V near 2135 UT. This peak is on the order of 10 to 15 mW/m^2. This is also the location of the strongest field-aligned current derived from the particles.

A more detailed examination of the particle, electric field, and magnetic field observations is summarized in Figure 3. This shows a schematic profile which represents UV auroral intensity versus universal time/ latitude. A time and latitude scale is shown on the horizontal axis so that the reader can refer back to Plates 2 and 3 with regard to the auroral and particle information. Figure 3 is divided into four panels each illustrating a particular set of Viking data. In order from top to bottom they show the patterns of aurora, electrons, ions, and the field-aligned currents/convection. A few of the more interesting points concerning this figure are listed below:

1. The most poleward ion precipitation is coincident with the most poleward arc system. This region has associated with it ion conics with peak energies less than about 2 keV.

2. The region 1 field-aligned current system (downward in the morning) is colocated with the most poleward ion precipitation. The sense of the field-aligned currents was derived from the change in the in situ magnetic field along the Viking trajectory. The convection reversal (westward to the north and eastward to the south) lies equatorward of these ions and the most poleward arc system of the double oval. This is based on electric field observations from the Viking spacecraft.

3. The strongest region 2 field-aligned current system (upward) originates between the two peaks in auroral intensity. It coincides with unstructured ion precipitation and structured electrons (inverted V's) less than about 1 keV.

4. The region of unstructured 1 to 10 keV electron precipitation overlaps with the structured electrons (less than 1 keV) and coincides with the main UV auroral oval.

5. Inverted V events occur near the peak in the main UV oval. Equatorward of this point the electron fluxes of plasma sheet energies begin to decrease with the higher energies disappearing first. In this region the isotropic boundary of energetic ions is found.

6. Low-energy ion dispersion signatures (LEIDS) can be seen in this most equatorward region. The dispersion signature seen here has the same sense as the most poleward velocity dispersed ion signature, that is, lower energies at lower latitudes. These occur just equatorward of the inverted V event.

7. A weak region 2 field-aligned current and eastward convective flow extend well equatorward of the main UV oval.

The CCE satellite was also traversing this region at high altitude between 1700 and 2300 UT. The trajectory of the satellite as it moved from L = 8.7 R_E to L = 1.7 R_E is shown in Plate 2 using two separate field line model projections for Kp = 3. The trajectory of CCE covers several hours and so the coordinates plotted are the magnetic coordinates of the points (i.e. the geographic points would rotate significantly relative to the aurora during this interval). The more poleward projection (white line) is due to the *Tsyganenko* [1987] model while the other (red line) is due to *Tsyganenko* [1989]. The points labeled 6 through 10 represent the CCE projections at 1910, 1930, 1940, 2120 and 2200 UT. Figure 4 shows the low-energy electron flux changes at four separate energy levels (1.8, 4, 9 and 20 keV) during this time interval. At the time when Viking traversed the auroral distribution, CCE encountered the inner portion of the central plasma sheet (2120 to 2150 UT).

The inner edge of the central plasma sheet will be considered to be the location at which plasma sheet electron fluxes dramatically decrease. Since this occurs at different locations for different particle energies, this edge is not a sharp one [*Fairfield and Vinas*, 1984]. The outer portion of this inner edge is the place at which the flux of particles with the highest energy shows a large decrease. The inner boundary is the point at which no plasma sheet particles of any energy are found. The inner edge of the plasma sheet is seen in the CCE data clearly between 2120 (point 9 in Plate 2) and 2200 UT (point 10). This region is extended in latitude and lies far equatorward of the main UV oval. It coincides in latitude to the region at Viking altitudes where only the more energetic trapped ions (> 20 keV) are seen. Before 2120 UT this inner edge is considerably more dynamic reflecting the active conditions. At about 1910 UT (point 6 in Plate 2), an injection of electrons from a distant source appears to take place with the 20 keV electrons becoming enhanced prior to the 9 keV electrons. These 20 keV fluxes subsequently decrease beginning about 1930 UT (point 7) followed by the 9 keV electrons at about 1940 UT (point 8). This dynamic region projects to the main UV auroral oval (points 6 to 8 in Figure 4b and Plate 2).

Interpretation and summary. Combining the information found in both the remote and in situ data two important relations can be found concerning the auroras during the expansion and recovery phases of a substorm:

1. The active region of the auroras during this expansion phase is located near the 40 keV isotropic proton boundary. This assumes that this boundary maintains its relationship to the main UV oval during this interval (a change of a degree or so is not important in the context of these particular images).

2. The active region of the auroras during this recovery phase is located near the poleward boundary of the plasma sheet particles. (It can be seen from the auroral data that this poleward boundary has not moved substantially over the interval in question).

The ion precipitation which shows an energy dispersion at the highest latitudes (2125 to 2128 UT) is similar to that reported by *Kovrazhkin et al.* [1987] and *Zelenyi et al.* [1990]. This VDIS has been associated with the plasma sheet boundary layer (PSBL) [e.g., *Kovrazhkin et al.*, 1987; *Zelenyi et al.*, 1990]. In the case presented here, however, it is coincident with the most poleward arc system. If, as others have done, we interpret this region as the ionospheric signature of the PSBL, then this region is also a source for auroral arcs. This differs from the view put forth by *Feldstein and Galperin* [1985] where the PSBL is a source for diffuse precipitation only. This point is further elaborated in the companion paper [*Elphinstone et al.*, 1994a].

The low-energy structured electron population just poleward of this ion precipitation is below the threshold of the UV imager. It is therefore unrelated to the UV polar arcs previously discussed in the context of being on closed field lines [e.g., *Elphinstone et al.*, 1993]. It is probably related instead to the weaker red line (6300 A) polar arcs which may occur on open field lines. This electron precipitation may come either

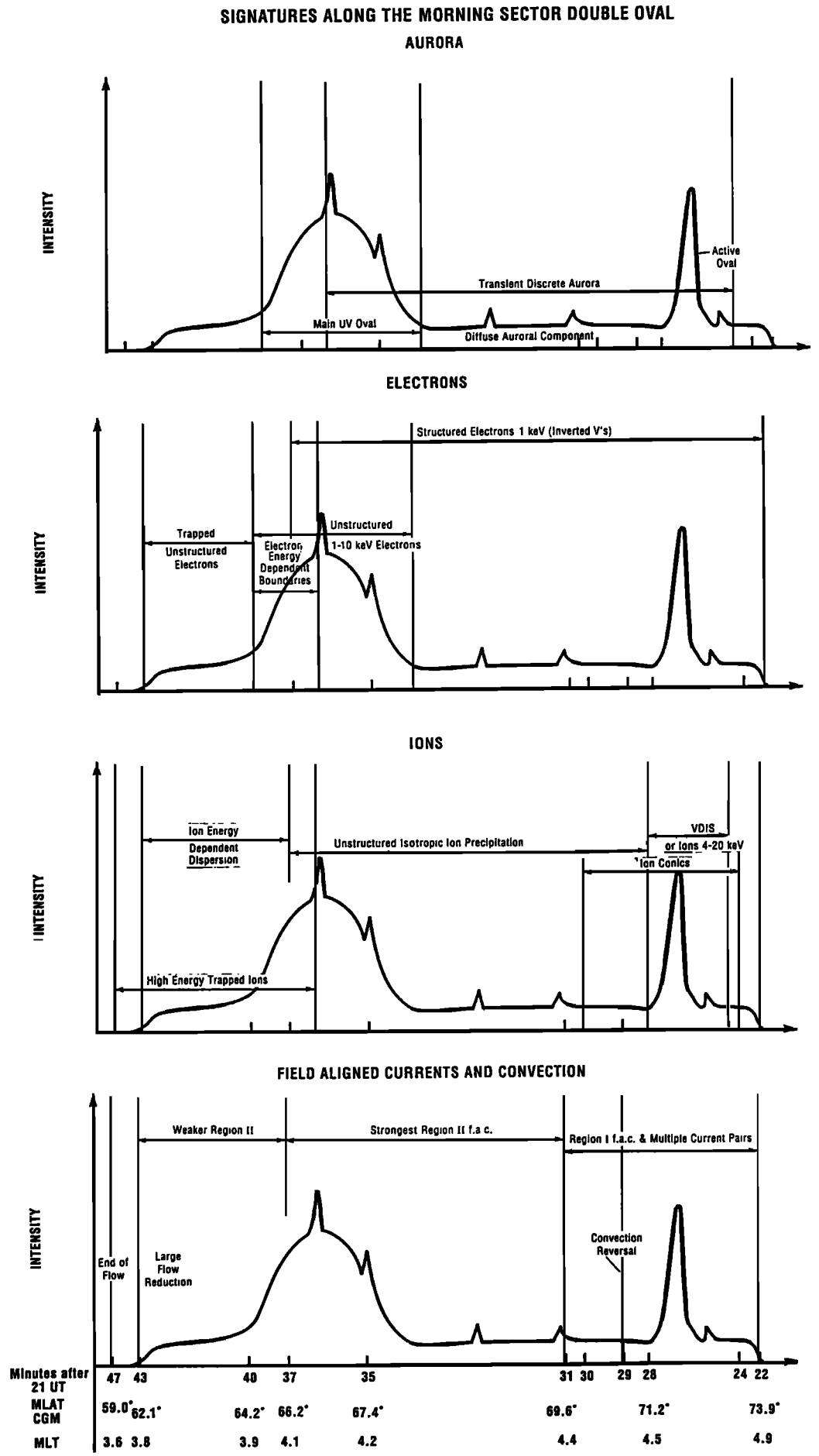
SIGNATURES ALONG THE MORNING SECTOR DOUBLE OVAL
AURORA
INTENSITY
Active Oval
Transient Discrete Aurora
Main UV Oval
Diffuse Auroral Component
ELECTRONS
INTENSITY
Structured Electrons 1 keV (Inverted V's)
Trapped Unstructured Electrons
Electron Energy Dependent Boundaries
Unstructured 1-10 keV Electrons
IONS
INTENSITY
Ion Energy Dependent Dispersion
Unstructured Isotropic Ion Precipitation
VDIS or Ions 4-20 keV
Ion Conics
High Energy Trapped Ions
FIELD ALIGNED CURRENTS AND CONVECTION
INTENSITY
Weaker Region II
Strongest Region II f.a.c.
Region I f.a.c. & Multiple Current Pairs
End of Flow
Large Flow Reduction
Convection Reversal
Minutes after 21 UT 47 43 40 37 35 31 30 29 28 24 22
MLAT CGM 59.0° 62.1° 64.2° 66.2° 67.4° 69.6° 71.2° 73.9°
MLT 3.6 3.8 3.9 4.1 4.2 4.4 4.5 4.9

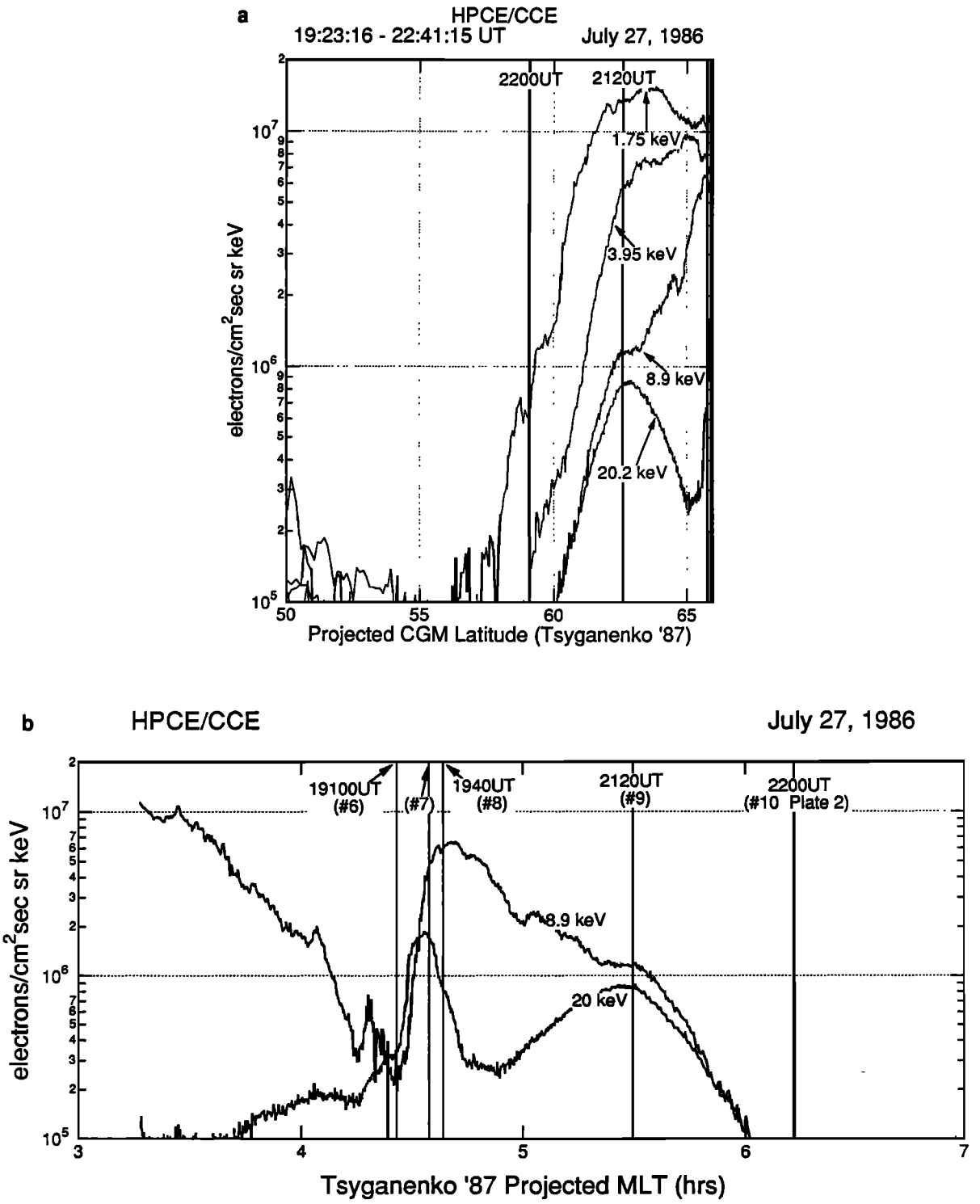

Figure 4. Electron fluxes at different energies recorded at the CCE satellite versus (a) projected T87 CGM latitude and (b) T87 CGM local time. The universal times marked correspond to the points shown in Plate 2. The main UV oval occurs near where the 20 keV fluxes peak.

Figure 3. (Opposite) Schematic of the morning sector double oval distribution illustrating the interrelationship between the various observations for the event shown in Plates 2 and 3. In order from top to bottom are the observations of the aurora, electrons, ions and field-aligned currents/convection. A schematic UV intensity contour is plotted in each panel as a reference.

from the deep tail low latitude boundary layer or the tail lobes and may be associated with the "warm envelope of the plasma sheet" found by *Zwolakowska et al.* [1992] with PROMICS-8 high-altitude data.

The region of unstructured 1 to 10 keV electron precipitation overlaps with the structured electrons (less than 1 keV) and coincides with the main UV auroral oval. Poleward of this region (2127 to 2137 UT) the ions show higher energies at lower latitudes characteristic of adiabatic acceleration in the plasmasheet [*Galperin et al.*, 1978; *Sauvaud et al.*, 1981; *Hardy et al.*, 1989]. Similar characteristics in the electrons could be interpreted as Fermi acceleration in the central plasma sheet. This result then links the results of *Sandahl and Lindqvist* [1990] and *Elphinstone et al.* [1991], who found each of these regions to map near the Earth.

The low-energy ion dispersion signatures (LEIDS) can be seen in this most equatorward region. These may be due to substorm injected ions or upflowing ions from the conjugate ionosphere which then separate under the influence of corotation, gradient and curvature drifts [*Sauvaud et al.*, 1981; *Winningham et al.*, 1984]. D. M. Klumpar et al. (Freja observations of ion dispersion precipitation signatures near the inner edge of the plasma sheet, submitted to *Geophysical Research Letters*, 1994) have associated these with the inner edge of the plasma sheet and, as in our case, also saw inverted V events just poleward of them. This region is associated with the equatorward portion of the main UV oval and lies equatorward of the 40 kev isotropic ion boundary. This again differs somewhat from the view put forth by *Feldstein and Galperin*, [1985] in that bright (in the UV at least) auroras are seen equatorward of this boundary. A weak region 2 field-aligned current and eastward convective flow extend well equatorward of the main UV oval. Two source regions (a near-Earth and tailward source) for region 1 field-aligned currents have previously been noted by *Ohtani et al.* [1988]. The results presented here tend to support that view.

Inverted-V events can be found close to the isotropic boundary of 40u keV ions in the morning sector. The results of *Lui and Burrows* [1978] and *Kirkwood and Eliasson* [1990] showed similar results for electrons. These inverted-Vs correspond with arcs on the main UV oval far equatorward of the most poleward arc system. The *Feldstein and Galperin* [1985] view that the discrete aurora maps to the central plasma sheet is supported by the results of this paper and the view that discrete aurora maps to the PSBL is also supported. Thus two important separate magnetospheric regions contribute to the discrete double oval auroral distribution. The low-energy electrons and protons which are presumably of plasma sheet origin show trapped fluxes which extend far equatorward of the main UV oval. Both the low- and high-altitude observations demonstrate that the inner edge of the plasma sheet is not a well-defined boundary but that it is in fact a magnetospheric region that maps to a latitudinally extended ionospheric region. Therefore it is not sufficient to simply state that something maps to the inner edge of the plasma sheet. The main UV oval where discrete arcs are found apparently coincides, at least at low altitudes, with the outer boundary of this region which appears to be quite dynamic.

Dayside and Evening Sector Double Ovals

Auroral distribution. The double oval distribution tends to occur predominantly in the morning sector but can be found to occur solely in the dusk sector or in both local time sectors simultaneously. Plate 4 shows the double oval distribution and its evolution over a 60-min time interval on July 27, 1986. This event occurred about 13 hours before the event discussed above. The AL index at this time varied between about 100 and 200 nT and was clearly recovering by 0800 UT. An auroral activation occurred at about 0715 UT which resulted in a double oval configuration by about 0730 UT. Between 0730 and 0800 UT, further auroral brightenings took place in the 21 to 0 MLT sector.

The left panel of Plate 4 shows an average auroral distribution covering an interval of time when DMSP-F7 flew over the northern evening sector distribution near 21 MLT (0738 to 0742 UT and labeled N1 in the plate) and over the dayside sector near 9 MLT (0729 to 0734 UT and labeled N2 in the plate). There was also an overflight of the dusk sector by DMSP-F6 between about 0731 and 0738 UT (labeled N3). The averaging was chosen to illustrate the auroral configuration during the passage of these satellites over the auroral regions. The change in the polar cap intensities from the top to the bottom of the images is due to changing solar zenith angle altering the dayglow intensities (the entire polar cap is sunlight for this event). The differences between the darkest regions in the left and right images of Plate 4 is an artifact of the scaling and averaging.

The main features of interest in the left panel are the following;

1. A double oval configuration is visible between 21 and 03 MLT. In this interval the main UV oval is the equatorward distribution while a second system is evident poleward of it. A minimum in intensity occurs between the two distributions although the intensity is not uniform with local time. The main UV oval extends continuously from the night sector to the dayside intensification near 15 MLT. The more poleward system does not extend to the dayside in the dusk sector.

2. A dawn sector Sun-aligned polar arc (i.e., aligned parallel to the 0 MLT meridian in the plate) is visible between 2 and 6 MLT. A fainter feature is also apparent which represents the weak extension of the double oval feature into the dawn sector. This feature becomes more clear in the subsequent panels.

3. Two arcs are visible between 6 and 9 MLT which are unconnected to the above mentioned features.

4. The afternoon peak intensity occurs near 15 MLT and there is a weak separate diffuse band of precipitation equatorward of this feature extending between 15 and 19 MLT.

The top right panel shows the average auroral configuration between 0811 and 0819 UT during the time period when DMSP-F7 flew over the southern evening sector (0815 to 0819 UT and labeled S2) and DMSP-F6 flew over the southern dusk sector aurora (0811 to 0815 UT and labeled S1). The plotted trajectories correspond to the southern hemisphere CGM coordinates at 120 km altitude plotted as northern hemisphere CGM coordinates. The mappings therefore assumed symmetric external current perturbations of the magnetic field about the equatorial plane (nonconjugate effects between hemispheres are due to asymmetric field perturbations between the north and the south). The changes which have occurred relative to the previous panel are given below:

1. The most poleward arc system of the double oval is somewhat less intense but now extends further into the dusk sector. This arc system has become a continuous arc system from about 18 MLT to at least 3 MLT.

2. There is a continuous arc on the main UV oval which begins near 18 MLT and extends to about 23 MLT. This arc system intensifies first near dusk and propagates rapidly eastward into the evening sector.

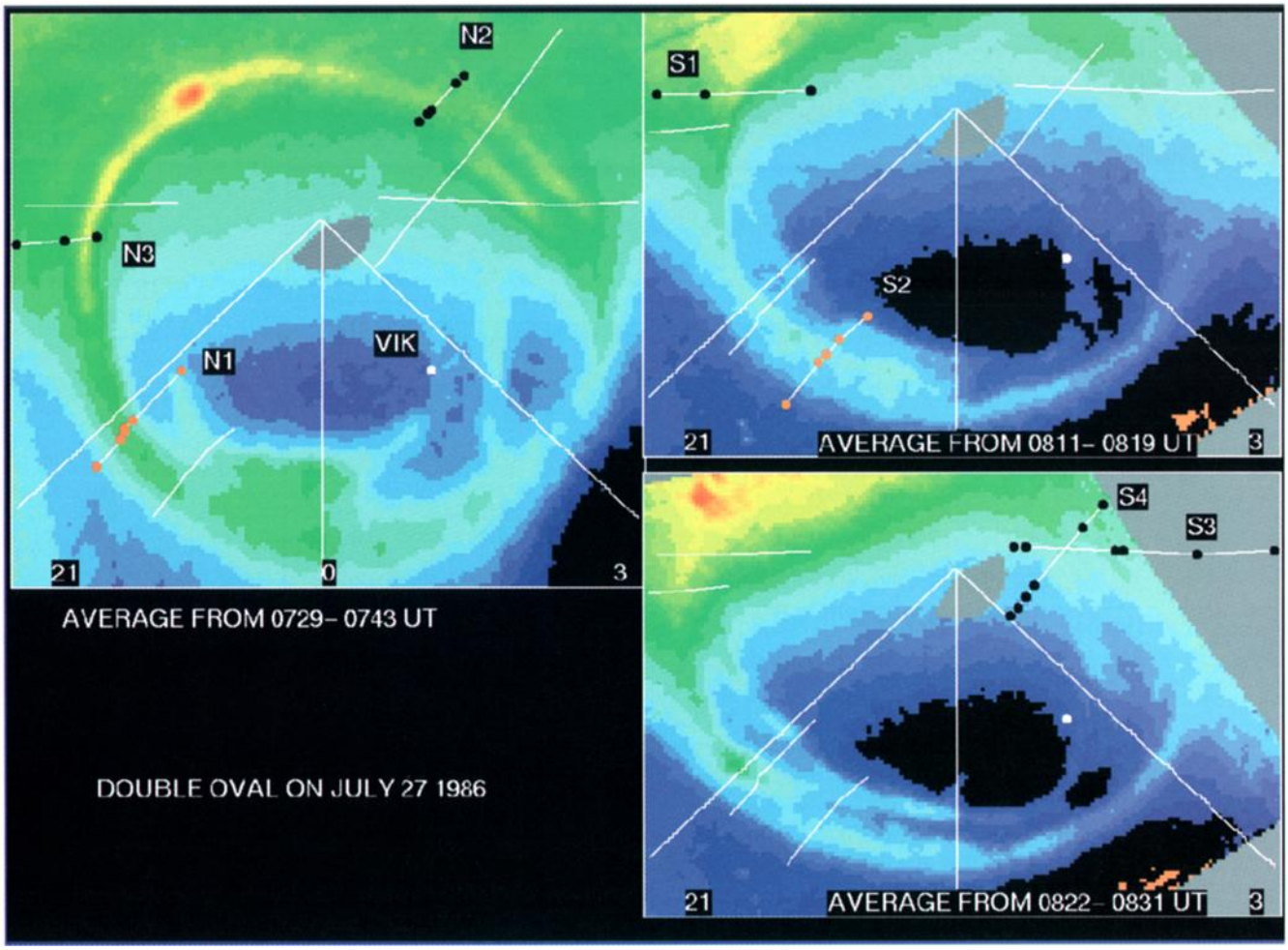

Plate 4. The double oval observed on July 27, 1986 between 0729 UT and 0831 UT. The intensities are represented by false colors ranging from dark blue (weakest) through yellow, red to white (most intense). DMSP trajectories S1 to S4 and N1 to N3 are shown and have the following neural network particle boundaries associated with them (beginning with the most poleward region and moving equatorward): N1- LABPS, LACPS, LABPS, LACPS, LABPS, LACPS; N2- Mantle, LLBL, LABPS, LACPS; N3- LABPS, LACPS; S1- LABPS, LACPS; S2- LABPS, LACPS, LABPS, LACPS; S3- LABPS, Void/Polar rain, Mantle; LABPS, LACPS; S4- LABPS, Void/Polar rain, LABPS, Void/Polar rain, Mantle. Dots have been used to separate the particle regions and have only been plotted in the panels corresponding to the UT range in which the particle observations occurred.

3. The Sun-aligned arc has disappeared or merged with the double oval configuration leaving only two regions of peak intensity. The double arc system in the late morning has also faded.

In the bottom right panel the auroral distribution is shown corresponding to the DMSP overflights in the late morning sector. The trajectory labeled S3 was a DMSP-F6 southern hemisphere pass between 0820 and 0827 UT, while S4 was a DMSP-F7 orbit from about 0823 to 0831 UT. This is also close to the time when Viking encountered the poleward boundary of about 5 keV ion precipitation near 3 MLT in the plate. The distribution in this case is similar to that seen between 0811 and 0819 UT except the following:

1. The most poleward system is more clearly visible near 7 MLT and near 19 MLT.

2. The arc system on the main UV oval has developed a spiral feature seen, in the Plate, as a green brightening near 21 MLT.

Although it may be obvious, it is perhaps useful to comment about the apparent lack of emissions between the two arc systems near 3 MLT in the panels on the right in Plate 4. This is not a true lack of UV emissions but is simply a result of the chosen intensity scale. A given color scheme is only able to resolve a certain intensity range. Thus in order to show the auroral distribution in full sunlight (the observations are in July in the northern hemisphere) a color scheme was chosen to enhance the global pattern. Naturally as a result, small scale variations are lost. It should not be taken to imply that the double oval distribution represents two systems separated by no emissions (see Figure 3).

Particles. The DMSP particle boundaries were determined by a neural network [see *Newell et al.*, 1991]. In what follows, the labels "LABPS" and "LACPS" have been used to identify traditional ionospheric particle regions known as boundary plasma sheet and central plasma sheet [*Winningham et al.*, 1975]. The prefix "low altitude" (LA) has been added to

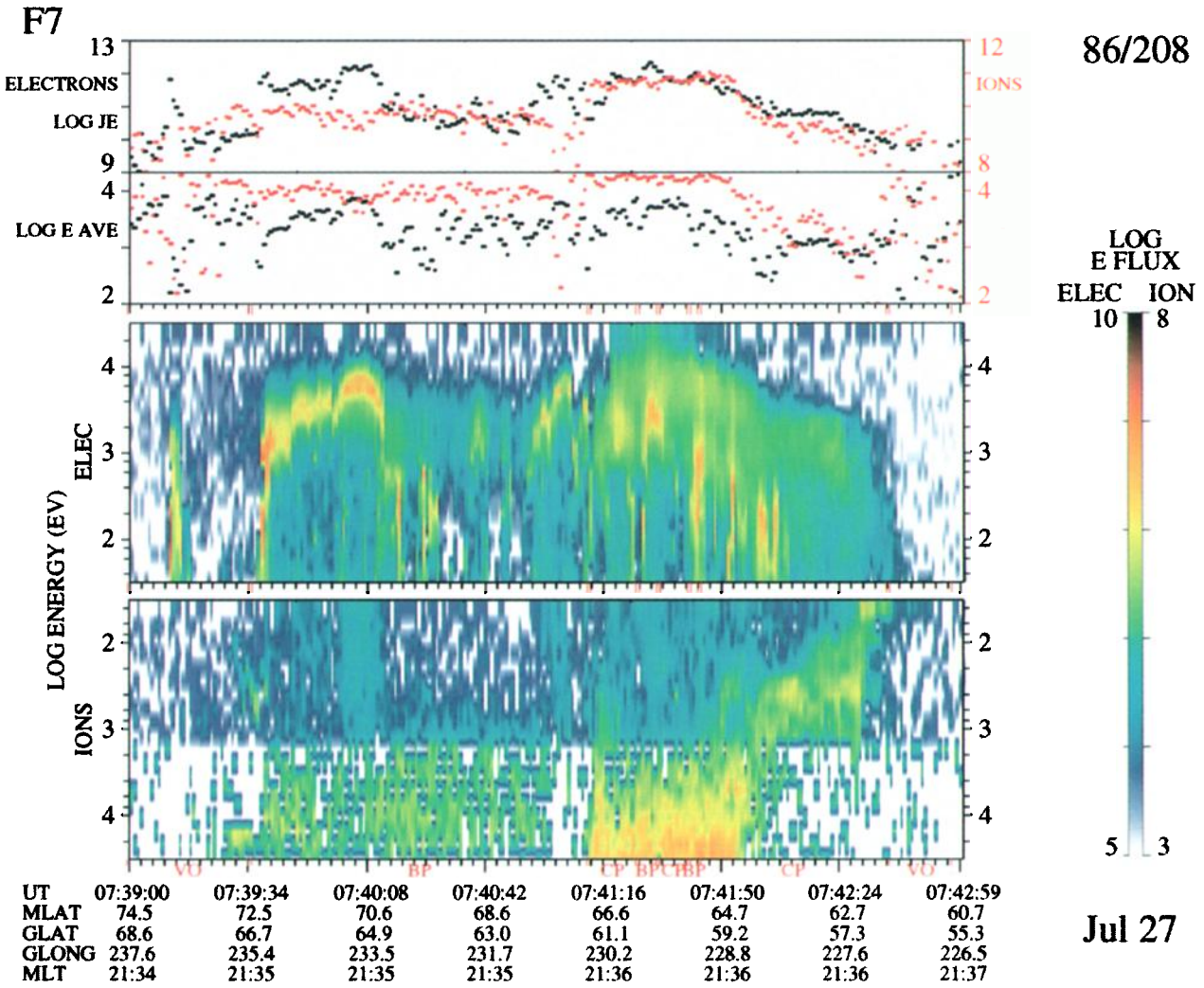

Plate 5. DMSP-F7 northern hemisphere spectrogram showing two sources of discrete auroral arcs. Electron/ion fluxes and energies are given in the top two panels while the bottom two panels show the time-energy spectrograms for ions and electrons. This spectrogram corresponds to the N1 trajectory shown in Plate 4.

these to ensure that the reader does not connect these with magnetospheric regions. In what follows the particle region definitions are based on neural network designations.

In each of the panels of Plate 4 all of the DMSP trajectories have been plotted as a reference to the reader. Those which occurred within the interval of time associated with a given panel have been plotted with dots. These dots delineate the various particle regions found by the neural network. The trajectories are the CGM 1980 coordinates of the DMSP orbit projected to 120 km altitude. For example the trajectories N1, N2, and N3 were northern hemisphere orbits by DMSP satellites which occurred within the time interval 0729 to 0743 UT.

The time-energy spectrogram for the N1 DMSP-F7 trajectory is shown in Plate 5. The double oval can clearly be made out as two regions of high electron flux (top panel of Plate 5) separated by a minimum near 0740 UT. Similar to the morning sector case, some low energy electrons were seen poleward of the main precipitation region (≈ 0739:15 UT). The most poleward LABPS region (0739:34 to 0741:12 UT) encompasses both the most poleward arc system and the region between the two ovals. This region had average ion and electron energies of 2.7 and 8.8 keV, respectively. Equatorward of this are four alternating regions of LACPS, LABPS, LACPS, and LABPS all located in the region of the main UV oval (the concentration of light red dots along the N1 trajectory represents this region). In the spectrogram this corresponds to the times from 0741:12 to 0741:41 UT. These regions show high fluxes of both electrons and ions relative to the more poleward region. The fluxes of ions increase with decreasing latitude. The average energy of the ions (12 to 16 keV) was higher through this region than the more poleward LABPS region. The electrons show higher average fluxes in the more equatorward LABPS regions. The most equatorward portion of the main UV oval was identified as LACPS. In this region, both the electrons (≈1 keV) and the ions (≈ 5 keV) have much lower average energies and fluxes. Again, similar to the morning sector, the energy of both the electrons and ions decreases with decreasing latitude.

A similar result is seen about 40 minutes later, one hour local time to the east near 22 MLT (profile S2 in the upper right panel). The most poleward arc system, and the poleward portion of the region between it and the main UV oval, were identified as LABPS. The arc system which has brightened on

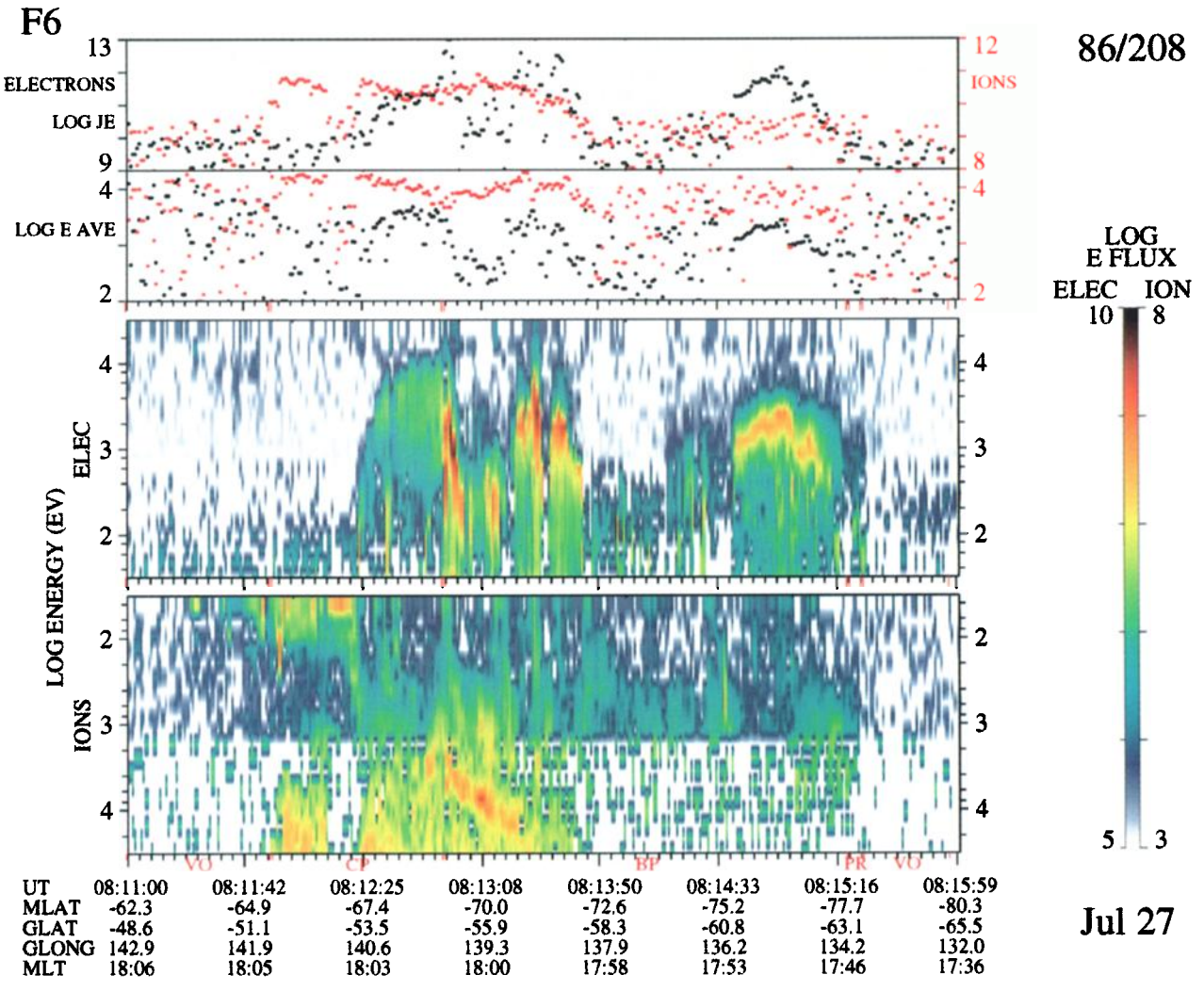

Plate 6. DMSP-F6 southern hemisphere spectrogram showing the dusk sector extension of the double oval configuration (same format as in Plate 5). A large flux decrease (top panel) is seen between the two arc systems. The most poleward system is not visible in the northern hemisphere UV auroral distribution. This spectrogram corresponds to the S1 trajectory shown in Plate 4.

the main UV oval is LABPS precipitation surrounded by LACPS precipitation. Here again we see the inverted V events embedded within a region of plasma sheetlike diffuse precipitation. The energies and fluxes of the particles follow similar trends to that described in the previous case. The most poleward arc in this case lies just equatorward of and adjacent to a velocity dispersed ion signature (VDIS). The point labeled "VIK" near 3 MLT in the left panel shows the location where the Viking spacecraft encounters the poleward edge of ions with energies of about 5 keV. This point coincides quite well with the poleward edge of the double oval configuration.

On the dayside and along the dawn/dusk meridian the situation is considerably different. What one sees is strongly local time dependent. The trajectory labeled "N2" in the upper left panel of Plate 4 has been investigated by *Ohtani et al.* [1995]. This showed an interesting set of four field-aligned currents in this sector associated with the two auroral arc systems located between 6 and 9 MLT. This DMSP orbit was just east of where the double oval could be seen and so registered a relatively standard set of dayside ionospheric particle boundaries. The most poleward region was mantle precipitation followed by low-latitude boundary layer and LABPS and LACPS in order as one moves equatorward on the trajectory (the dots delineate the boundaries of the regions). Similarly, near 18 MLT, the trajectory labeled N3 (0736-0738 UT) in the upper left panel of Plate 4 also showed nothing unusual with the poleward region being LABPS and the more equatorward region identified as LACPS. Note that the LABPS region is located on the same arc system which is associated with the equatorward LABPS found closer to midnight in the N1 trajectory. The LACPS region at this local time is associated with a separate detached portion of auroral emission. The particle characteristics of this trajectory look similar to those found on the nightside.

The particle characteristics however change in the dusk sector by the time of the southern hemisphere overflight (S1 in the top right panel). The time-energy spectrogram for the S1 trajectory is shown in Plate 6. The top panels show how the ion and electron average energies and fluxes change and it is clear that there is a dramatic depletion in the electron flux and energy between the two sets of arcs at about 0813:20 and

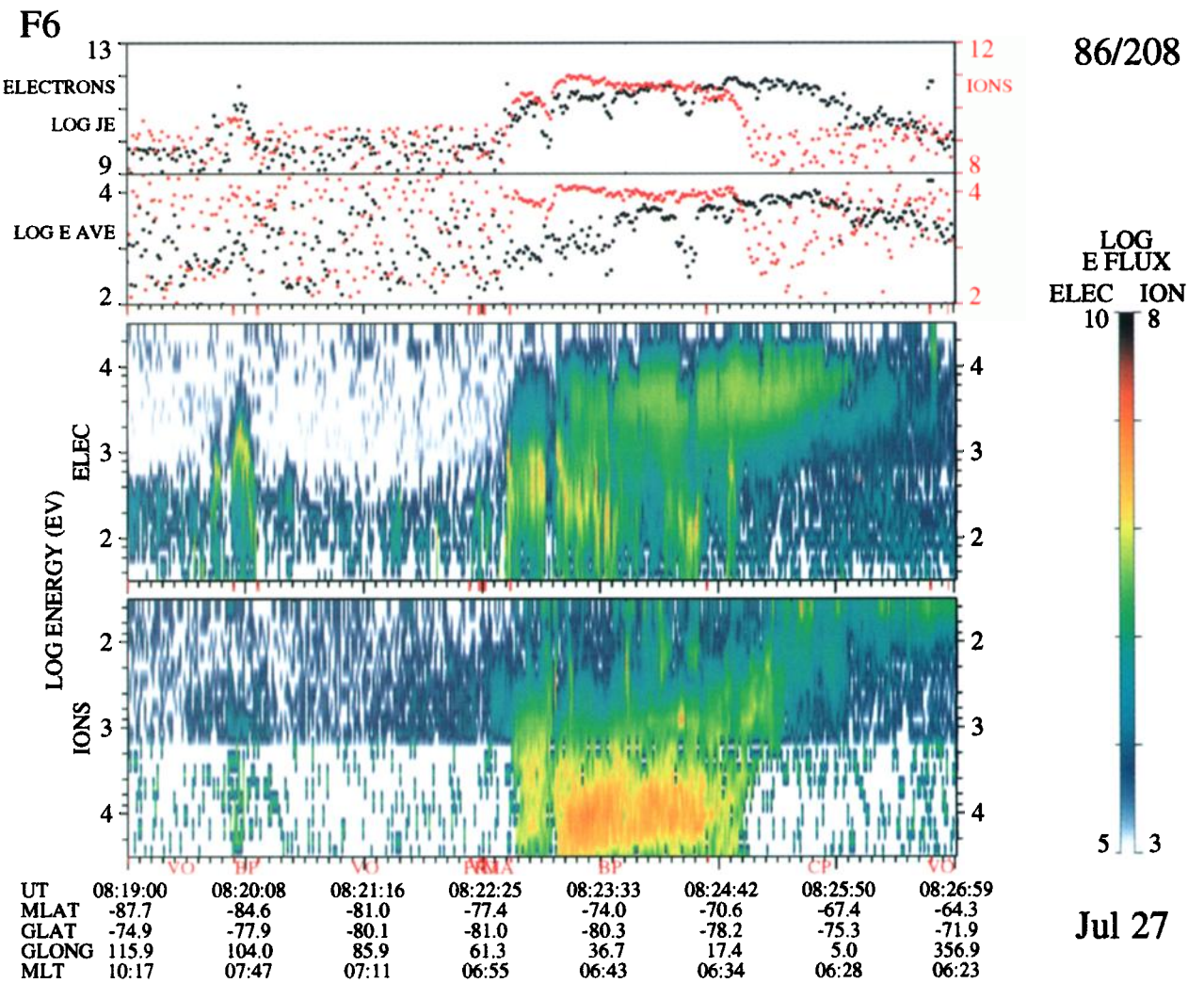

Plate 7. DMSP-F6 southern hemisphere spectrogram (same format as Plate 5) showing the various particle regions associated with the dayside extension of the double oval configuration. This spectrogram corresponds to the S3 trajectory shown in Plate 4.

0814:50 UT. There is a second similar depletion at about 0813:00 UT. The more poleward arc feature was not evident some 40 minutes previously in the northern hemisphere (N3). This appears to be the extension of the most poleward arc system of the double oval configuration into the dayside ionosphere. Note that in this case, there was no obvious UV signature of the most poleward arc system at this local time in the northern hemisphere. The more equatorward set of arcs were associated with ions whose energy decreased with decreasing latitude.

The morning sector also had interesting signatures associated with the extension of the double oval into the dayside region. Further to the west of the N2 trajectory two southern hemisphere DMSP passes (S3 and S4) took place between 0822 and 0831 UT. The dots on the S4 pass separate the following regions as one moves equatorward: LABPS, void/polar rain, LABPS, polar rain and mantle precipitation. Similarly for S3 the regions are: LABPS, void/polar rain, mantle, LABPS, and LACPS. The time energy spectrogram for the S3 pass is shown in Plate 7. The above mentioned regions are marked on the Plate. What is immediately evident from Plate 7 is the arc system near 0820 UT which lies about 7 degrees poleward of the main precipitation region. This constitutes the dayside extension of the double oval configuration.

The regions of LABPS, void/polar rain and mantle line up rather well for these two DMSP passes indicating the two-dimensional character of the different precipitation regions. There is a general correspondence between the the most poleward arc system of the double oval and the LABPS signatures although the lack of exact correspondence is probably due to a lack of conjugacy of these high latitude arcs between the north and the south. These DMSP LABPS regions have a lower electron average energy than is usually seen on the nightside or on the more equatorward LABPS. For the S3 pass the average energy was only 0.3 keV, while for S4 the two most poleward LABPS signatures had average energies of 0.6 and 0.9 keV. The region classified as void/polar rain by the neural network is associated with a depletion between the double ovals and the mantle region appears towards the poleward boundary of what one might describe as the main UV oval at these local times. This identification of mantle by the neural network is probably not accurate and could probably be re-labeled as LABPS since the average ion energy of 3.5 keV is rather high for mantle precipitation. It and the electron energies were, however, consid-

erably lower than the region of LABPS immediately equatorward.

Interpretation and summary. During the first part of this event (0729 to 0743 UT) the double oval was active in a region limited to 6 hours of local time centred around midnight. DMSP satellite passes during this interval confirm this and show two separate regions of LABPS-like precipitation in the evening sector. The more poleward region was associated with the discrete aurora at the poleward edge of the double oval as well as weaker features in the region between the two ovals (similar to the top of Figure 3). The more equatorward region lay embedded within a LACPS particle region. The existence of the discrete aurora in this region again supports the view of *Feldstein and Galperin* [1985] and is contrary to the view that this region is always purely diffuse precipitation.

The S2 DMSP pass showed that the discrete arcs near the poleward boundary lay equatorward of and adjacent to what one might consider to be the ionospheric signature of the Plasma Sheet Boundary Layer (i.e., the VDIS). This contrasts with the morning sector event which showed these features to be coincident. It therefore appears that this most poleward arc system can be associated with either the PSBL itself or with its inner edge. What governs this relationship is probably related to local conditions within the boundary layer itself.

On the other hand, the inner portion of the central plasma sheet is frequently associated with only diffuse precipitation at low altitude. We have, however, seen two cases where discrete auroral forms are embedded within this inner region. *Galperin et al.* [1992] have presented a means by which these arc systems might form in this inner region. In the next section we give an example in which this inner region makes a transition from diffuse to discrete.

We have also seen the signatures of the double oval in the dawn and dusk sectors to be considerably different than those seen closer to midnight. These arc systems form in association with the substorm process [*Elphinstone et al.*, 1993] and form a continuous feature from midnight to the dayside. Although they have the particle characteristics of the PSBL on the night-

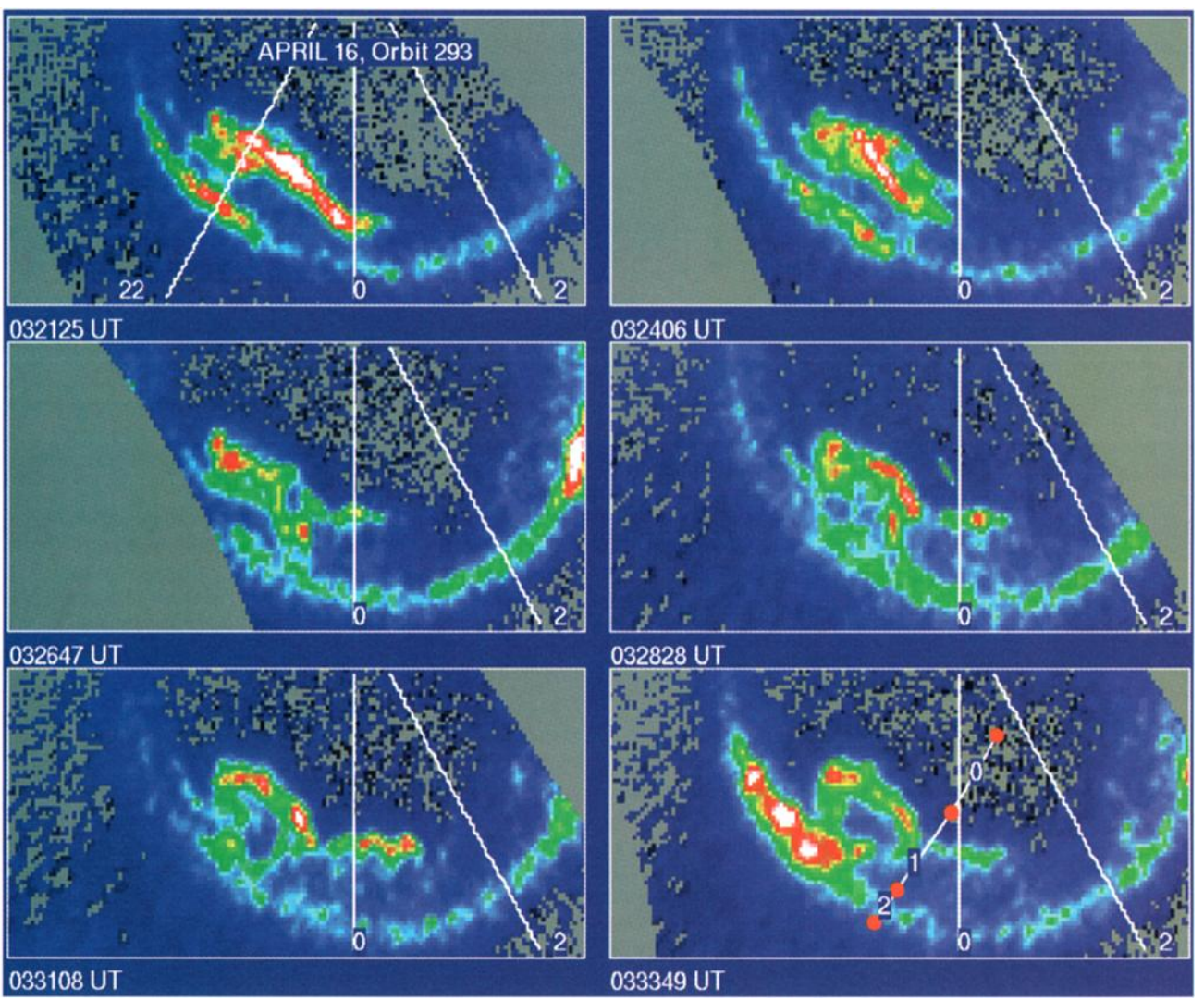

Plate 8. The coupling of the two portions of the double oval. Viking images are shown from 0321 to 0334 UT on April 16, 1986. Points along the DMSP-F7 satellite trajectory are shown in the lower right panel to illustrate the the various low altitude particle regions relative to the auroral distribution. Regions 0, 1, and 2 correspond to no precipitation, LABPS and LACPS respectively. An arc system can be seen to begin from the most poleward oval (top right panel) and propagate toward the main UV oval. It couples to the main UV oval by about 0331 and 0334 UT an azimuthal auroral form intensifies on the main UV oval.

side, they resemble the signatures of polar arcs on the dayside (see, for example, the the polar arc observations by *Burch et al.* [1992]). We suggest that the dayside portion of the double oval maps to the deep tail flanks of the magnetosphere, as was proposed for polar arcs by *Elphinstone et al.* [1993]. The particle signatures equatorward of these arcs is dependent on whether the Low Latitude Boundary Layer earthward of the source is on overdraped open field lines or not [see *Elphinstone et al.*, 1994]. This in turn depends on the the sense of the y component of the interplanetary magnetic field.

This mapping scheme allows the double oval to be continuous from midnight to the dayside. It interprets the changing particle characteristics as being due to a change in source region from PSBL to LLBL, and explains the ionospheric signatures using a magnetospheric topology which is simple. This is the only method known to us which also explains as a natural consequence the Sun-aligned nature of the polar arcs and the features of the double oval configuration.

4. Coupling of the Two Auroral Distributions

Plate 8 shows how a coupling can exist between the most poleward auroral arc system and the main UV auroral oval. At 0321 UT in the top left panel of Plate 8 a single arc system on the most poleward oval can be seen between about 21 and 0 MLT. By 0324 UT a new system has penetrated the region between the two ovals and is aligned from the northwest to the southeast. At this time it is still connected to the most poleward system. In the next panel at 0326:47 UT this arc system can be seen more clearly and now extends almost to the main UV oval. It creates a north-south aligned connection between the two ovals. By 0328:28 UT the emissions in the main UV oval connect to the feature and by 0331:08 UT it has faded but the main UV oval to the west has brightened somewhat. A substorm onset then begins from this location (lower left panel).

The activation at 0333 UT occurs on the main UV oval at a time when the more poleward system is active and a large scale stationary surge exists (see, for example, the image in the lower left panel). There was a DMSP-F7 overflight of the region just to the east of the activation region between 0332 and 0336 UT. The various particle regions as defined by the neural network have been delineated in the panel at 0331 UT. In this case the LACPS corresponds closely to the location of the main UV oval where the new activation occurs. This illustrates an important aspect of these particle definitions. A new discrete auroral activation has occurred in a region of LACPS.

Interpretation

This is an example of a disturbance that was probably initiated in the PSBL and eventually after about 10 min generated conditions in the near-Earth region sufficient to begin a near-Earth substorm onset. *Baker et al.* [1993] have previously attributed near-Earth onsets to triggering due to reconnection earthward of x_{GSM} = -25 R_E. Our results indicate that the coupling may be somewhat indirect, such that the propagation inward allows the triggering of an onset in the inner region of the magnetosphere. This type of coupling appears to be sufficient but not necessary for a near-Earth onset.

Associated with the onset arc would be conditions such that parallel potential drops could be set up and the aurora becomes more dynamic. This occurs in a region which was previously diffuse and LACPS-like in character. This transition of the main UV auroral oval from a diffuse to discrete character is fundamental to understanding the substorm onset as having a near-Earth source.

This is supported both by the observation that the poleward arcs remain poleward of the new system and by the observations given in Plates 2 and 4 showing the discrete arcs embedded within the diffuse LACPS-like region. The "variance image" results shown in Plate 2 (event A) further support this view and indicate that different regions of the ionosphere/magnetosphere system become active during the expansion phase and recovery phase. We can now begin to understand the dynamics of the region named by *Winningham et al.* [1975] as the collapsing BPS. This is the region between the two "ovals" which can develop field-aligned potential drops and form dynamic arc systems in a previously inactive diffuse auroral area. To understand this region properly a more global view must be adopted and the dynamics of the region evaluated. It will also be important in the future to distinguish between the two types of discrete precipitation which are associated with each oval in the double oval configuration.

These dynamics allow one to reconcile two competing views about the origin of auroral arc systems. Frequently, the only discrete arcs originate in or near the PSBL. Under other conditions (which are not yet clear) the inner magnetosphere becomes an active source region for these arcs. This can happen at substorm onset but also can continue well into substorm recovery. One important question to address in the future is whether the inner magnetosphere is a source for arcs under very quiet conditions and what magnetospheric conditions give rise to them.

5. Summary and Conclusions

The double oval distribution forms at the beginning of substorm recovery (or end of the expansion phase) and plays an integral part in understanding subsequent auroral activations. The more equatorward oval or the main UV oval is a steady feature of the auroral distribution in contrast with the more poleward one. This main UV oval in the morning sector is located near the isotropic boundary of 40 keV ions and substorm onset is associated with it.

The poleward oval begins to develop at the end of expansion phase and dependent on conditions can develop during substorm recovery phase into a distribution covering most magnetic local times. Particle data support the linkage of the poleward oval to boundary layer processes which become active during substorm recovery phase. This most poleward system near midnight shows periodic activations which can develop into large scale surge forms. This poleward oval can be linked to PSBL processes near midnight but is more easily explained as being a deep tail low latitude boundary layer phenomenon closer to the dayside. There appears, therefore, to be an interesting transition region somewhere between 18 and 21 MLT (and also 03 to 06 MLT) where the most poleward arc ceases to have PSBL characteristics and takes on the character associated with high latitude polar arc events. This view then separates the ionospheric projection of the deep tail low latitude boundary layer and the plasma sheet boundary layer and puts constraints on substorm theories.

Observations were given which show that a coupling can occur between the near-Earth substorm onsets and processes originated in the PSBL. These observations show that the tem-

poral development of features during the double oval configuration are fundamental to understanding the LABPS and LACPS signatures which result from local satellite observations. As arcs develop in the inner magnetosphere, in association with substorm onset, regions of overlapping discrete and diffuse auroras occur in the ionosphere. This helps one to understand controversies which have arisen concerning the mapping of auroral arcs. Two fundamentally different source regions for nightside discrete auroral arcs appear to exist for magnetically active conditions.

To investigate the dynamics of the nightside substorm region we have developed a new technique for the analysis of auroral image data. This uses what we have called "variance images" to produce images of the active and dynamic regions of the aurora. These indicate that fundamentally different regions can be active during the expansion and recovery phases of a substorm.

Acknowledgements. The authors would like to thank Ann Marie Morris for helping with the manuscript. The Viking project was managed by the Swedish Space Corporation under contract to the Swedish Board for Space Activities. The UV imager was built as a project of the National Research Council of Canada and this work was supported under grants from Natural Sciences and Engineering Research Council of Canada. A. Wright is supported by a United Kingdom PPARC Advanced Fellowship. The Lockheed portion of this work was supported by NASA contract number NAS5-30565. The first author would like to thank T. Lui for suggestions and a valuable evaluation of the paper and one referee for suggesting changes which have greatly helped the paper.

The Editor thanks T. I. Pulkkinen and another referee for their assistance in evaluating this paper.

References

Baker, D. N., T. I. Pulkkinen, R. L. McPherron, J. D. Craven, L. A. Frank, R. D. Elphinstone, J. S. Murphree, J. F. Fennell, R. E. Lopez and T. Nagai, CDAW 9 analysis of magnetospheric events on May 3, 1986: Event C, *J. Geophys. Res., 98*, 3815-3834, 1993.

Burch, J. L., N. A. Saflekos, D. A. Gurnett, J. D. Craven, and L. A. Frank, The quiet time polar cap: DE 1 observations and conceptual model, *J. Geophys. Res., 97*, 19,403-19,412, 1992.

Burke, W. J., J. S. Machuzak, N. C. Maynard, E. M. Basinska, G. M. Erickson, R. A. Hoffman, J. A. Slavin, and W. B. Hanson, Auroral ionospheric signatures of the plasma sheet boundary layer in the evening sector, *J. Geophys. Res., 99*, 2489-2499, 1994.

Craven, J. D., and L. A. Frank, Latitudinal motions of the aurora during substorms, *J. Geophys. Res., 92*, 4565-4573, 1987.

Cogger L. L. and R. D. Elphinstone, The Viking auroral substorm, International Conference on Substorms - 1, Kiruna, Sweden, *Eur. Space Agency Spec. Publ., SP-335*, p. 77-82, 1992.

Elphinstone, R. D., D. J. Hearn, J. S. Murphree, and L. L. Cogger, Mapping using the Tsyganenko long magnetospheric model and its relationship to Viking auroral images, *J. Geophys. Res., 96*, 1467-1480, 1991.

Elphinstone, R. D., and D. J. Hearn, Mapping of the auroral distribution during quiet times and substorm recovery, International Conference on Substorms - 1, Kiruna, Sweden, *Eur. Space Agency Spec. Publ., SP-335*, 13-18, 1992.

Elphinstone, R. D., J. S. Murphree, D. J. Hearn, W. Heikkila, L. L. Cogger, and I. Sandahl, The auroral distribution and its mapping according to substorm phase, *J. Atmos. Terr. Phys., 55*, 1741-1762, 1993.

Elphinstone, R. D., et al., The double oval UV auroral distribution, 2, The most poleward arc system and the dynamics of the magnetotail, *J. Geophys. Res.*, this issue.

Elphinstone, R. D., D. J. Hearn, and J. S. Murphree, Dayside aurora poleward of the main auroral distribution: Implications for convection and mapping, in *Physical Signatures of Magnetospheric Boundary Layer Processes*, edited by J. A. Holtet and A. Egeland, pp. 189-200, Kluwer Academic, Norwell, Mass., 1994.

Fairfield, D. H., and A. F. Vinas, The inner edge of the plasma sheet and the diffuse aurora, *J. Geophys. Res., 89*, 841-854, 1984.

Feldstein, Y. I., and Y. I. Galperin, The auroral luminosity structure in the high-latitude upper atmosphere: Its dynamics and relationship to the large scale structure of the Earth's magnetosphere, *Rev. Geophys., 23*, 217-275, 1985.

Galperin, Y. I., V. A. Gladyshev, N. V. Jorjio, R. A. Kovrazhkin, V. M. Sinitsin, F. Cambou, J. A. Sauvaud, and J. Crasnier, Adiabatic acceleration induced by convection in the plasma sheet, *J. Geophys. Res., 83*, 2567-2573, 1978.

Galperin, Y. I., A. V. Volosevich, and L. M. Zelenyi, Pressure gradient structures in the tail neutral sheet as roots of the arcs with some effects of stochasticity, *Geophys. Res. Lett., 19*, 2163-2166, 1992.

Hardy, D. A., M. S. Gussenhoven, and D. Brautigam, A statistical model of auroral ion precipitation, *J. Geophys. Res., 94*, 370-392, 1989.

Kamide, Y., and S-I. Akasofu, The auroral electrojet and global auroral features, *J. Geophys. Res., 80*, 3585-3602, 1975.

Kirkwood, S., and L. Eliasson, Energetic particle precipitation in the substorm growth phase measured by EISCAT and Viking, *J. Geophys. Res., 95*, 6025-6037, 1990.

Kovrazhkin, R. A., J. M. Bosqued, L.. M. Zelenyi, and N. V. Georgio, Observation of evidence of reconnection and plasma acceleration at a distance of about 5 x 10^5 km in the tail of the Earth's magnetosphere, *JETP Lett., 45*(8), 479-482, 1987.

Kotikov, A. L., A. V. Frank-Kamenetsky, Yu. O. Latov, O. A. Troshichev, E. M. Shishkina, J. S. Murphree, and R. D. Elphinstone, Filamentary structure of the westward electrojet in the midnight sector auroral distribution during substorms: Comparison with Viking auroral observations, *J. Atmos. Terr. Phys., 55*, 1763-1774, 1993.

Lui, A. T. Y., D. Venkatesan, C. D. Anger, S.-I. Akasofu, W. J. Heikkila, J. D. Winningham, and J. R. Burrows, Simultaneous observations of particle precipitations and auroral emissions by the Isis 2 satellite in the 19-24 MLT sector, *J. Geophys. Res., 82*, 2210-2226, 1977.

Lui, A. T. Y., and J. R. Burrows, On the location of auroral arcs near substorm onsets, *J. Geophys. Res., 83*, 3342-3348, 1978.

Lyons, L. R., Association between tail substorm phenomena and magnetic separation distortion, in *Magnetospheric Substorms, Geophys. Monogr. Ser.*, vol. 64, edited by J. R. Kan et al., pp. 161-170, AGU, Washington, D. C., 1991.

Murphree, J. S., C. D. Anger, and L. L. Cogger, ISIS-2 observations of auroral arc systems, in *Physics of Auroral Arc Formation, Geophys. Monogr. Ser.*, vol. 25, edited by S.-I.

Akasofu and J. R. Kan, pp. 15-23, AGU, Washington, D. C., 1981.

Murphree, J. S., and R. D. Elphinstone, Correlative studies using the Viking imagery, *Adv Space Res., 8*, 9-19, 1988.

Nakamura, R., T. Oguti, T. Yamamoto, and S. Kokobun, Equatorward and poleward expansion of the auroras during auroral substorms, *J. Geophys. Res., 98*, 5743-5759, 1993.

Newell, P. T., S. Wing, C.-I. Meng, and V. Sigillito, The auroral oval position, structure, and intensity of precipitation from 1984 onward: An automated on-line data base, *J. Geophys. Res., 96*, 5877-5882, 1991.

Nielsen, E., et al., Oval intensification event observed by stare and Viking, *J. Geophys. Res., 98*, 6163-6171, 1993.

Ohtani, S, S. Kokubun, R. C. Elphic, and C. T. Russell, Field-aligned current signatures in the near-tail region, 1, ISEE observations in the plasma sheet boundary layer, *J. Geophys. Res., 93*, 9709-9720, 1988.

Ohtani, S., et al., Four large-scale field aligned current systems in the dayside high-latitude region, *J. Geophys. Res., 100*, 137-153, 1995.

Pellinen, R. J., H. J. Opgenoorth, and T. I. Pulkkinen, Substorm recovery phase: Relationship to next activation, International Conference on Substorms - 1, Kiruna, Sweden, *Eur. Space Agency Spec. Publ., SP-335*, 469-475, 1992.

Sandahl, I., and P.-A. Lindqvist, Electron populations above the nightside auroral oval during magnetic quiet times, *Planet. Space Sci., 38*, 1031-1049, 1990.

Sauvaud, J. A., J. Crasnier, K. Mouala, R. A. Kovrazhkin, and N.V. Jorjio, Morning sector ion precipitation following substorm injections, *J. Geophys. Res., 86*, 3430-3438, 1981.

Sergeev, V. A., T. Bosinger, R. D. Belian, G. D. Reeves, and T. E. Cayton, Drifting holes in the energetic electron flux at geosynchronous orbit following substorm onset, *J. Geophys. Res., 97*, 6541-6548, 1992.

Tsyganenko, N. A., Global quantitative models of the geomagnetic field in the cislunar magnetosphere for different disturbance levels, *Planet. Space Sci., 35*, 1347-1358, 1987.

Tsyganenko, N. A., A magnetospheric magnetic field model with a warped tail current sheet, *Planet. Space Sci., 37*, 5-20, 1989.

Winningham, J. D., F. Yasuhara, S.-I. Akasofu, and W. Heikkila, The latitudinal morphology of 10-eV to 10-keV electron fluxes during magnetically quiet and disturbed times in the 2100-0300MLT sector, *J. Geophys. Res., 80*, 3148-3171, 1975.

Winningham, J. D., J. L. Burch, and R. A. Frahm, Bands of ions and angular V's: A conjugate manifestation of ionospheric ion acceleration, *J. Geophys. Res., 89*, 1749-1754, 1984.

Zelenyi, L. M., R. A. Kovrazkhin, and J. M. Bosqued, Velocity dispersed ion beams in the nightside auroral zone: Aureol 3 observations, *J. Geophys. Res., 95*, 12,119-12,140, 1990.

Zwolakowska, D, P. Koperski, and B. Popielawska, Plasma populations in the tail during northward IMF, International Conference on Substorms - 1, Kiruna, Sweden, *Eur. Space Agency Spec. Publ., SP-335*, 57-62, 1992.

L. L. Cogger, R. D. Elphinstone, D. J. Hearn, J. S. Murphree, Department of Physics and Astronomy, University of Calgary, Calgary, AB, Canada T2N 1N4.

D. M. Klumpar, Space Science Laboratory, Lockheed Missiles and Space Co. Inc., Palo Alto, CA 94304.

K. Mursula, Department of Physical Sciences, University of Oulu, Oulu, SF 90570 Finland.

P. T. Newell, S. Ohtani, and T. A. Potemra, Applied Physics Laboratory, Johns Hopkins University, Laurel, MD 20723.

I. Sandahl, Swedish Institute for Space Physics, S981 28 Kiruna, Sweden.

J. A. Sauvaud, Toulouse University, BP 4346, 31029 Toulouse, France.

M. Shapshak, Institute of Plasma Physics, Kungliska Tekniska Hogskolan, 100 44, Stockholm, Sweden.

A. Wright, Mathematical Institute, University of St. Andrews, St. Andrews KY16 9SS, Fife, Scotland.

(Received July 25, 1994; revised January 24, 1995;
accepted January 24, 1995.)